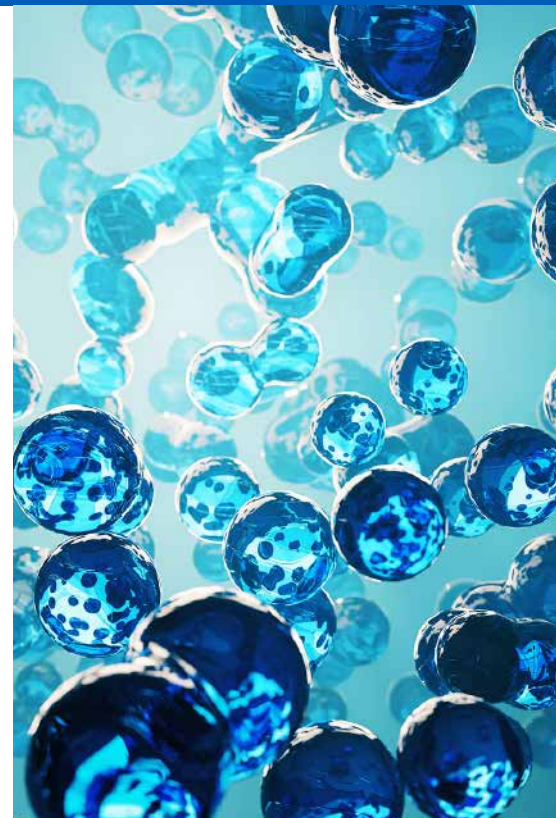


11

Advanced Optical Metrology

Particles II



Contents

- 3 Introduction

- 6 A new method of imaging particle tracks in solid-state nuclear track detectors
D. Wertheim, G. Gillmore, L. Brown, N. Petford

- 13 Application of confocal microscopy for surface and volume imaging of solid-state nuclear track detectors
D. Wertheim, G. Gillmore

- 19 Application of confocal microscopy for 3D visualization of tracks in solid-state nuclear track detectors
D. Wertheim, G. Gillmore

Imprint

© Wiley-VCH GmbH
Boschstr. 12,
69469 Weinheim, Germany
Email: info@wiley-vch.de
Editor-in-Chief: Dr. Christina Poggel

The Impact of Particles on Biological Systems and the Environment

Particles with their unique properties are used in numerous applications, such as for electronic devices, pharmaceuticals, and energy materials, just to name a few. In addition, in the "Advanced Optical Metrology: Particles I" eBook, it is described how liquid crystalline elastomer (LCE) particles can be magnetically remote controlled and used as transport systems. When combined with Fe_3O_4 , these nanoparticles have the potential to transport plastic, textiles, and copper, enabling novel LCE applications, such as micro-robots controlled by magnetism.



Figure 1: Nano- and microparticles are distinctive materials with enormous technological and scientific value.

The benefits of micro- and nanoparticles are extensive, ranging from treating new diseases to increasing storage energy capacity in batteries. Particle research is generating millions of dollars of revenue, especially in the fields of medicine, energy, and food safety. However, one disadvantage of these particles is their often poor degradability, making them a potential problem for humans, animals, and the environment. This eBook is dedicated to the research of David Wertheim, Professor at Kingston University London; in collaboration with different groups, Prof. Wertheim is using confocal microscopy to analyze the impact of different types of particles on human health and the environment. Herein, the focus lies on his research on particles hazardous to human health detected with solid-state nuclear track detectors (SSNTD).

INTERACTION OF PARTICLES WITH BIOLOGICAL SYSTEMS

Numerous research groups around the world are investigating the impact of micro- and nanoparticles on biological and ecological systems. Both synthetic micro- and nanoparticles, as well as particles resulting from the degradation of waste or emissions, are studied. Some of the results are so shocking that even the daily press reports on them. For example, researchers found that plastic particles can be found everywhere in the world, from Mount Everest^[1] to

the Mariana Trench^[2]. Recently, microplastics were even detected in human blood^[3].

At the nanoscale, nanoparticles can physico-chemically interact with organic chemicals or metals present in the environment; this interaction may alter their bioavailability and result in mixture effects, such as synergism, antagonism, and addition. The different effects are not only dependent on the properties of individual components but also on environmental conditions and biological systems^[4].

One of the main mechanisms of interaction between inorganic nanoparticles and environmental components is adsorption^[5-7]. The adsorption of contaminants onto nanoparticles can occur in two ways: as a facilitator in delivering contaminants, where the nanoparticles act as a carrier increasing the uptake by the organisms^[8] — a process known as the “trojan horse effect” — and as a reducer of the concentration of contaminants in the environment, either by strong absorption or aggregation/sedimentation, decreasing the co-contaminant mobility and bioavailability^[9].

Learn more about the application of confocal microscopy for 3D imaging of particulate matter in a recent presentation by **Prof. David Wertheim** and **Dr. Gavin Gillmore**.



AIR POLLUTION PARTICULATE MATTER

Exhaust fumes caused by traffic are a major health concern, especially in densely populated areas. In many countries, there are upper limits for fine dust values that are regularly exceeded despite stricter regulations for particulate filters in diesel vehicles. To understand how diesel particulates enter the body and interact with cells, a detailed understanding of the properties of the particles is necessary.

Air pollution particulate matter is the subject of Prof. David Wertheim's current work, which he is conducting in collaboration with researchers at Queen Mary University of London, UK. In a study published in 2021, they used a new color confocal microscope imaging method to study the 3D shape of diesel particulate matter^[10]. They found that the particles adhere to human lung epithelial cells, which is in line

Figure 2: Microplastics are a major problem for the aquatic ecosystem.





Figure 3: Fine dust pollution in cities harms people and the environment.

with their findings that they can have sharp jagged appearing edges. With the new findings of this study, the researchers are helping to explain why air pollution particulate matter can enter cells of the human respiratory tract, causing various health problems, including neurological and cardiovascular diseases.

SOLID-STATE NUCLEAR TRACK DETECTORS

Small etched plastic detectors, so-called solid-state nuclear track detectors (SSNTD), can be used to monitor radon levels. This is important for the safety of workers exposed to radon at their workplace, as inhalation of radon gas has been linked to the development of lung cancer. In several studies presented in this eBook, Prof. David Wertheim and colleagues have been working to further develop this method using confocal microscopy.



© David Wertheim

DAVID WERTHEIM

David Wertheim is a Professor in the School of Computer Science and Mathematics at Kingston University London, UK. The main focus of his research is developing methods for analysis and visualization of medical, biological, and material image and signal data; a key area of his current research is the acquisition and analysis of confocal microscope images of particulate matter.

REFERENCES

- [1] I. E. Napper et al., *One Earth* (2020) 3, 621–630.
- [2] X. Peng et al., *Geochem. Persp. Let.* (2018) 9, 1–5.
- [3] H. A. Leslie et al., *Environment International* (2022) 163, 107199.
- [4] Y. Liu, Y. Nie, J. Wang, J. Wang, X. Wang, S. Chen, G. Zhao, L. Wu, A. Xu, *Mechanisms involved in the impact of engineered nanomaterials on the joint toxicity with environmental pollutants*, *Ecotoxicol. Environ. Saf.* 162 (2018) 92–102, <https://doi.org/10.1016/j.ecoenv.2018.06.079>.
- [5] Krzyżewska, Iwona, et al. "Inorganic nanomaterials in the aquatic environment: behavior, toxicity, and interaction with environmental elements." *Archives of Environmental Protection* 42.1 (2016).
- [6] Li, Mengting, Wei Liu, and Vera I. Slaveykova. "Effects of mixtures of engineered nanoparticles and metallic pollutants on aquatic organisms." *Environments* 7.4 (2020): 27.
- [7] Bushra, Rani, Anees Ahmed, and Mohammad Shahadat. "Mechanism of adsorption on nanomaterials." *Advanced Environmental Analysis*. 2016. 90–111.
- [8] K.A. Heys, R.F. Shore, M.G. Pereira, K.C. Jones, F.L. Martin, *Risk assessment of environmental mixture effects*, *RSC Adv.* 6 (2016) 47844–47857, <https://doi.org/10.1039/c6ra05406d>.
- [9] M. Li, W. Liu, V.I. Slaveykova, *Effects of mixtures of engineered nanoparticles and metallic pollutants on aquatic organisms*, *Environments* 7 (2020) 1–20.
- [10] Miyashita, Lisa, Foley, Gary, Gill, Ian, Gillmore, Gavin, Grigg, Jonathan and Wertheim, David (2021) *Confocal microscopy 3D imaging of diesel particulate matter*. *Environmental Science and Pollution Research*, 28, pp. 30384–30389.

01 A new method of imaging particle tracks in solid-state nuclear track detectors

D. Wertheim, G. Gillmore, L. Brown, *et al.*

SUMMARY

Solid-state nuclear track detectors are used to determine the concentration of α particles in the environment. The standard method for assessing exposed detectors involves 2D image analysis. However, 3D imaging has the potential to provide additional information relating to angle as well as to differentiate clustered hit sequences and possibly energy of α particles, but this could be time-consuming. Here, we describe a new method for rapid, high-resolution 3D imaging of solid-state nuclear track detectors. A LEXT™ OLS3100 confocal laser scanning microscope (Olympus Corporation, Tokyo, Japan) was used in confocal mode to successfully obtain 3D image data on four CR-39 plastic detectors. Three-dimensional visualization and image analysis enabled the characterization of track features. This method may provide a means of rapid and detailed 3D analysis of solid-state nuclear track detectors.

INTRODUCTION

Inhalation of radon gas (^{222}Rn) and associated ionizing decay products is known to cause lung cancer in humans^[1,2]. In the United Kingdom, it has been suggested that 3–5% of total lung cancer deaths can be linked to elevated radon concentrations in the home and/or workplace. Radon monitoring in buildings is therefore routinely undertaken in areas of known risk. Indeed, some organizations such as the Radon Council in the United Kingdom and the Environmental Protection Agency in the United States, advocate a ‘to test is best’ policy^[3]. Radon gas occurs naturally, emanating from the decay of ^{238}U in rock

and soils. Measurement of radon in the environment is important in order to give appropriate warning of potential risks, for example in mines and homes, as well as to establish where remedial action is required^[4,5,6,7].

Radon gas concentration can be measured using CR-39 plastic detectors^[7], which conventionally are assessed by 2D image analysis of the surfaces. It is important to note that there can be some variation in reported results, even in closely spaced detectors^[8], due in part to error margins in measurement equipment or techniques. We have previously observed that radon tracks in CR-39 detectors can be visualized using confo-

cal microscopy and hence information about 3D track geometry can be obtained^[9].

A number of radon measurement methods are currently in use (e.g., activated carbon and electrets) but the most widely used are CR-39 solid-state nuclear track-etch detectors. In this technique, heavily ionizing α particles leave tracks in the form of radiation damage (via interaction between α particles and the atoms making up the CR-39 polymer). Typically, two CR-39 plastic detectors are installed in a building over a 3-month period, one in the lounge and one in the bedroom of a domestic property, following Health Protection Agency (HPA) protocols^[7]. After exposure, in the United Kingdom, the detectors are then sent to an HPA-accredited laboratory for processing. As the latent tracks are not visible under an optical microscope, chemical etching must be performed. This is usually done by etching the detector in a caustic soda (NaOH) bath for 4 hours, after which time the surface pitting made by α particles is revealed. The etch pits can then be counted using a microscope, allowing the radon concentration to be computed (based on the number of tracks for a given area on the detector surface). Where the Radon Metrology Laboratory is concerned at Kingston University (an HPA-accredited laboratory and the source of our detectors in this study), this is carried out by an automated RadoSys microscope/computer system. A number of internationally regulated counting methods have been set up for analyzing radon exposure using passive detectors^[10]. The majority use a combination of optical microscopes, spark counters, and computer-based image scanning and processing systems. The etching characteristics of solid-state nuclear track-etch detectors, in particular CR-39-type plastics, are well known from experimental studies, where track evolution with etching follows a well-defined geometry^[11].

Some tracks may be at an angle, resulting in variation in gray levels seen in microscopy^[12]. Our study extends earlier work^[9], which was aimed at classifying and quantifying the shape, size, area, and angular distribution of nuclear tracks in solid-state detectors. Such analysis forms the basis of the fission track dating method^[13]. It has been highlighted that it is necessary to count the number of naturally occurring and induced tracks in order to determine the uranium content of the material, to produce fission track-based ages^[14]. Induced tracks are formed by irradiating the sample in contact with an external detector,

generally a low-uranium mica or a CR-39-type plastic, where induced fission of ^{235}U produces tracks in the detector that can be revealed subsequently by chemical etching.

The track structure of α particles in CR-39 is different from that in crystals^[9]. However, there are similarities to radon monitoring in that detectors are chemically etched to reveal and count fission tracks under an optical microscope. Where fission track dating is concerned, it is possible to incorrectly estimate the age of a sample through track loss. For example, shallow angle tracks may not be fully revealed by chemical etching and/or may not be counted correctly. It has been suggested that confocal microscopy may provide a way of quantifying this track loss^[9].

AIM

The aim of this study was to acquire and analyze high-resolution 2D and 3D image data of etched radon tracks in CR-39 detectors.

MATERIAL AND METHODS

A LEXT™ OLS3100 confocal laser scanning microscope (Olympus Corporation, Japan) with a 408 nm laser was used in order to acquire images of four etched CR-39 radon detectors. In this study, two objective lenses (50X and 100X) were used for the collection of 3D data, both having a numerical aperture of 0.95. The manufacturer's user manual (version 5) indicates that the microscope has a planar resolution of up to 0.12 μm (using the 100X objective) and a height resolution of up to 0.01 μm . The detectors from the Radon Metrology Laboratory at Kingston University were put on a glass slide, which was then placed on the microscope stage.

Acquisition and analysis of 2D surface images

In this study, 2D surface images of the detectors, obtained with a 10X objective, were analyzed. With the 10X objective lens, each pixel corresponded to 1.25 μm . A charge-coupled device is used to acquire 2D color images from reflected light. The maximum number of pixels per field of view using the charge-coupled device camera (optical) is 1024 x 768. Images of the central portion of the detectors were processed using software we developed at Kingston University using MATLAB (The MathWorks, Inc., Natick, MA, U.S.A.).

The color images (.bmp files) were converted to gray scale and then binary following manual entry of an appropriate threshold value; using the software small objects in the resultant binary image were removed and a 3 x 3 median filter was applied. Appropriate detection of the radon tracks could be checked from an image obtained by superimposing a contour of the detected tracks onto the gray scale or color image, and hence, the suitability of the threshold could be visually assessed. Tracks near the edge of the image were not included in case they were not complete. The detected objects were then analyzed using the 'regionprops' function in MATLAB; this method is similar to that previously described^[9]. The area, perimeter, and shape of the tracks were assessed. In addition, the images were visually examined in order to investigate the possible occurrence of closely spaced tracks. Tracks were identified visually on the light white background as dark round or elliptically shaped objects that may have a pale center.

Acquisition and analysis of 3D images

The LEXT microscope was used in confocal mode in order to acquire 3D image data of more than 60 tracks of which 51 were single tracks. The height of the top surface and the deepest track were manually determined in order to allow the image data to be acquired over an appropriate depth range.

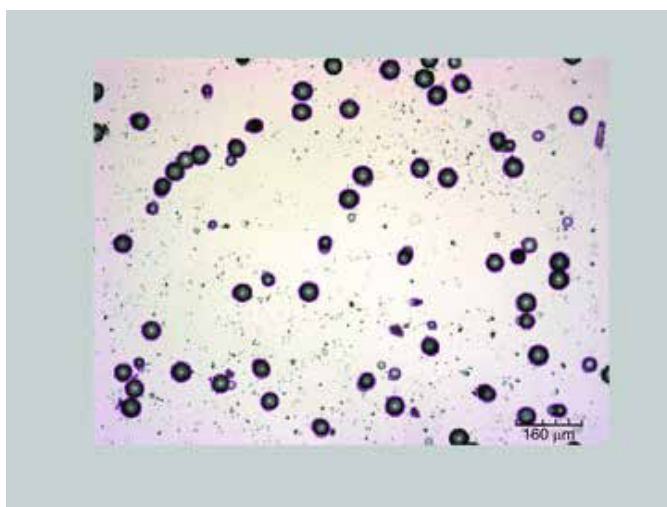


Figure 1: Image showing segmentation of tracks (shown in purple) on an image using a 10X objective. The tracks are seen as darker elliptical or circular areas. A range of track sizes and gray levels is seen as well as some overlapping tracks. The long rectangular object on the upper right is assumed to be an artifact and was thus not included in the analysis.

For this study, a 50X objective was used for the initial 3D examination of the detectors as this appeared to give an appropriate level of detail for the tracks while allowing several tracks to be imaged. The movement between each step in the z-direction was 180 nm for the 50X objective and 50 nm for the 100X objective. For the 50X objective lens, each pixel corresponds to 0.25 μm . In order to view further surrounding tracks, the tiling feature was used to acquire a series of adjacent images which were then stitched together; the stitching involves a 15% overlap of the adjacent tiled images. The 3D visualizations were compared with 2D surface images.

The 3D data, including height information, was visualized and analyzed using the LEXT system. Hence the depth profile and changes in gray level were examined in tracks that appeared to be inclined, as identified by an elliptical cross-section, by manually selecting cross-sections through the visualization of the tracks. We also investigated possible connections between tracks when there were closely spaced multiple events. Data with height information was also exported to a spreadsheet-compatible file so that it could be visualized with additional software we developed using MATLAB.

RESULTS

A total of 229 single tracks or clusters of multiple tracks (range 53 to 63 per detector) were seen in the images of the four detectors. An example of an image of tracks and their detection is shown in **Figure 1**. There were 182 clear single tracks, 25 double adjacent tracks, and 7 regions of apparently more than 2 adjacent tracks; there were a further 15 single or double tracks where there appeared to be some artifacts and hence were not included in the following analysis. The area data for the single tracks was not consistent with a normal distribution using the Ryan-Joiner test in MINITAB v. 15 (Minitab, Inc. State College, PA, U.S.A.), and hence median, quartiles, and range are used for the descriptive statistics. The area, perimeter, equivalent diameter, roundness, and eccentricity of the single and double radon tracks are shown in **Table 1**.

Eccentricity is the ratio of the distance between the foci of the ellipse divided by the length of the major axis; thus, for a circle the value is 0. The eccentricity values suggest that most of the single tracks are elliptical, which

Single tracks	Minimum	Q 1	Median	Q 3	Maximum
Area (μm^2)	315.63	1228.13	1668.75	1898.13	3062.50
Equivalent diameter (μm)	20.05	39.54	46.10	49.16	62.44
Perimeter (μm)	64.63	128.89	152.05	161.31	213.56
Major axis length (μm)	21.44	43.45	48.78	51.00	75.79
Minor axis length (μm)	14.33	35.75	43.99	48.35	54.59
Roundness	0.97	1.06	1.09	1.13	1.70
Eccentricity	0.04	0.24	0.37	0.57	0.89

Double tracks	Minimum	Q 1	Median	Q 3	Maximum
Area (μm^2)	1067.19	2348.44	3078.13	3448.44	4384.38
Equivalent diameter (μm)	36.86	54.69	62.60	66.26	74.71
Perimeter (μm)	124.98	200.31	241.24	265.24	356.78
Major axis length (μm)	47.09	68.01	86.09	98.83	126.94
Minor axis length (μm)	29.26	43.81	47.83	50.72	55.15
Roundness	1.15	1.28	1.41	1.66	2.31
Eccentricity	0.61	0.78	0.83	0.87	0.92

Table 1: Minimum, Q1, median, Q3, and maximum values of area, perimeter, roundness, and other measures for single and double tracks.

is consistent with visual observation. Using Spearman's rank correlation there is a significant negative correlation between area and eccentricity ($r=0.541$, $n=182$, $P < 0.001$), although there was wide variation when examining the data with a scatter plot.

Compactness is defined as the ratio of perimeter squared divided by area^[15] and roundness is that ratio divided by 4π ^[16]. Thus, a circle has the lowest roundness of 1. In this data, all

the objects had a roundness of 1 or more except for one very small object (222 pixels in area) with a measured roundness value of 0.97. The median roundness of the single tracks of 1.09 is also consistent with many tracks not being exactly circular in cross-section.

Three-dimensional visualization helps in investigating variation in area and depth as well as identifying coalescing tracks as seen in **Figure 2** where a 50X objective was used. The

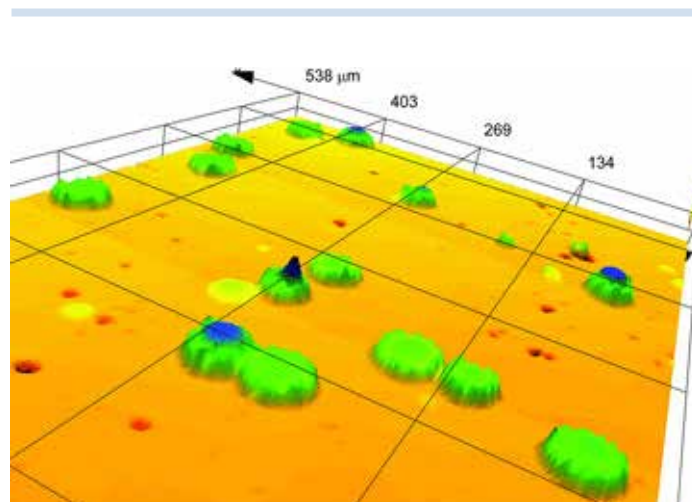


Figure 2: Example of 3D visualization of tracks from data obtained with a 50X objective showing the distribution of tracks in the 3×3 stitched area; some adjoining tracks can be seen. The color coding shows the height: red being the top, through yellow, blue, green, and to purple being the deepest.

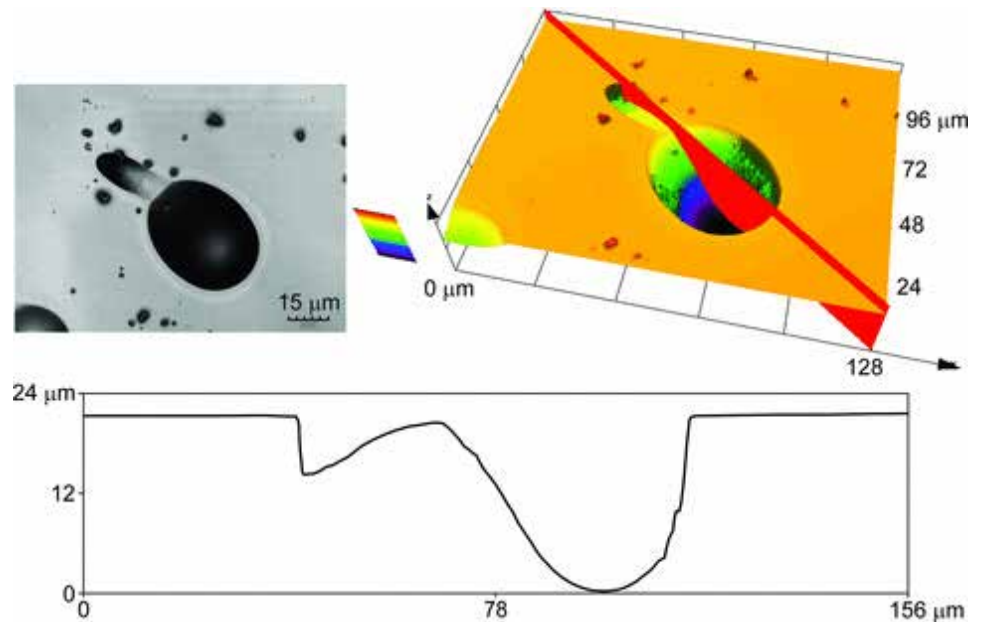


Figure 3: An example showing two tracks in 2D together with a depth-encoded color image and the profile through the tracks that were taken with a 100X objective. As in **Figure 2**, the color coding shows the height: red being the top, through yellow, blue, green, and to purple being the deepest. The gradient profile suggests that the left track was formed by an α particle coming from the right side, whereas the larger right-hand track appears to have been formed by a particle from the left-hand side as the slope is seen to be less steep.

examples in **Figures 2** and **3** show that track areas appear to be highest at the surface and become smaller going deeper into the detector. The 3D image data in **Figure 2** was exported to a spreadsheet file in order to enable the analysis of the track area using additional software developed using MATLAB (The MathWorks, Inc.) at Kingston University. The software detects the surface layer and hence can identify tracks emanating down from the top surface. From the 3D image data, the area of nine single tracks at the detector surface was analyzed and compared with a corresponding 2D image acquired with a 10X objective. The mean (standard deviation) difference in the track area, (3D – 2D measurements) divided by the mean of the 2D and 3D area, was 5.1% (4.2%); this data was consistent with a normal distribution using the Ryan–Joiner test in MINITAB v. 15 (Minitab, Inc.) and using a one-sample t-test were significantly different from 0 ($P = 0.008$).

Acquisition of each 3D dataset (without tilting) takes typically about 5 minutes depending on settings; 130 steps can be scanned per minute in the z-direction when using any of the objectives. Visualization and basic anal-

ysis of the 3D track data typically takes less than 10 minutes, depending on the size of the image and the type of analyses performed. Some of the observed elliptical shape tracks were associated with different gradients on either side of the corresponding depth profile of the 3D data. From the profile graph in **Figure 3**, the deeper track can be seen to have a depth of about 22 μm whereas the shallow track has a depth of about 10 μm . An indication of the track angle can be derived from the depth and spatial position data. The gradient of the profile is likely to indicate the angle at which the α particle hit the detector; two examples of this are seen in **Figures 3** and **4**, which also show that 3D visualization and depth profiles can help in understanding the relative size and angles of a sequence of multiple hits from the way in which the tracks are formed (**Figure 4**). The profile graph in **Figure 4** shows clearly the depths of the two tracks on the right are about 18 and 22 μm . In addition, in the example in **Figure 4**, the outline 2D shape suggests there may be two tracks, whereas the greater detail from 3D visualization shows that there are three tracks.

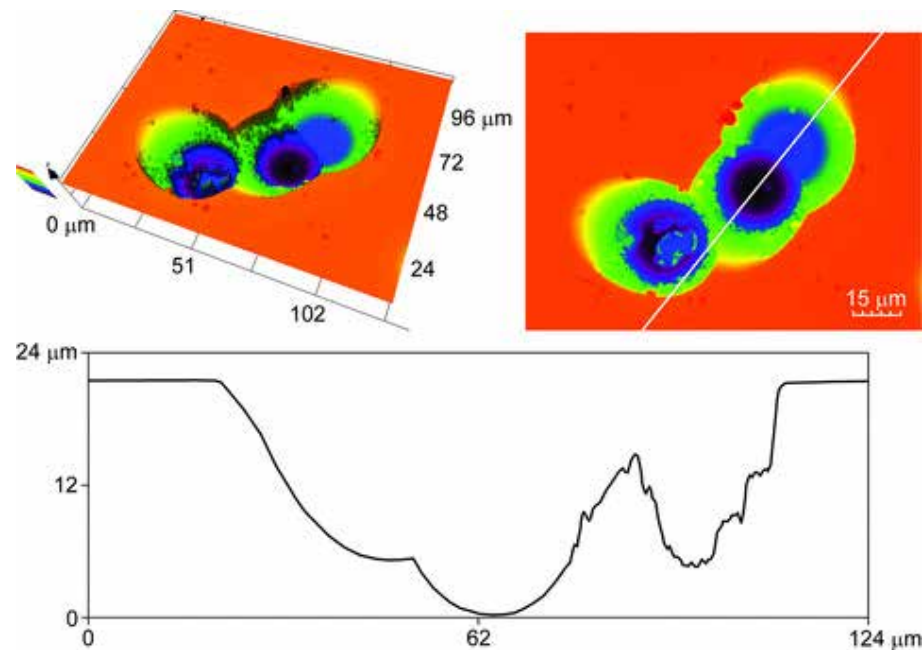


Figure 4: An example of multiple coalescing tracks obtained with a 100X objective. The profile of this image is shown just below and confirms that the tracks are individual overlapping tracks with the middle track being the deepest. The height color coding is as in **Figures 2 and 3**. The white line through the image shows where the profile map has been taken.

DISCUSSION

In this study, clear visualizations of surface and 3D tracks were obtained and a number of patterns such as single, double, and multiple hits as well as angled hits were observed. Further to our earlier paper^[9], in this investigation, 3D images of the full depth of tracks together with greater detail were obtained. The lower wavelength laser as well as the 50X and 100X objective lenses used here for 3D microscopy contribute to the improved resolution. Hence, it was possible to visualize in detail the occurrence of angled tracks in 3D and to quantify the angle along different profile lines; such visualization allows assessment of the direction in which the α particles collide with the detector. From the 2D image data, the area of tracks shows marked variation, and preliminary results suggest that this may be inversely related to the eccentricity, which is consistent with visual observations that lower area tracks appeared to be more elliptical in shape. It would be interesting to investigate if area is related to the angle of inclination. The 50X objective used for 3D dataset collection enables higher spatial resolution images than the 10X objective

and hence correspondingly influences track area measurement accuracy. Measurements of surface track area obtained from a 3D image using the 50X objective were found to be similar to corresponding area measurements from a 2D image using the 10X objective; the mean difference observed was 5.1% which, albeit small, was significantly different from 0 ($P = 0.008$). The higher track area, observed using 3D imaging, is likely to be due to the decrease in the area seen going deeper into the detector. For 2D imaging, this may result in less contrast around the circumference of the track, which thus could affect the area detected when applying the thresholding algorithm.

The variability of radon track measurements from 2D measurements may in part be due to the difficulty of selecting true tracks from an artifact. It was observed that high-resolution 3D visualization can help in accurately identifying tracks and quantification of their geometry. Although collecting 3D datasets takes more time than conventional 2D imaging, the 3D data enables further analysis of tracks than from 2D data alone; this should help in better understanding track formation and more

precise determination of the number of radon tracks. For example, multiple closely spaced tracks could be due to hits from multiple particles or possibly bouncing of particles on the detector surface; 3D imaging should enable the distinction of particle bouncing from multiple particle hits by assessment of the depth and angle data. The occurrence of areas of adjacent multiple hit tracks was observed; the reason for α particles appearing to impinge on the detector more often in certain areas is unclear, but it is possible that the process of track formation causes a change in surface charge. In summary, high-resolution 3D images of radon tracks in CR-39 plastic detectors obtained using confocal microscopy in combination with 2D microscope images enable detailed analysis of their physical dimensions and shape; the full depth of tracks and their angle with respect to the surface could be quantified. The techniques described in this study allow detection of tracks of different sizes and may thus help to improve the accuracy and repeatability of radon measurements as well as gain a better understanding of track formation.

REFERENCES

- [1] Darby, S., Hill, D., Auvinen, A., et al. (2005) Radon in homes and risk of lung cancer: collaborative analysis of individual data from 13 European case-control studies. *BMJ*. 330, 223–226.
- [2] ICRP (International Commission on Radiological Protection) (2007) Recommendations of the International Commission on Radiological Protection. ICRP publication 103. *Ann. ICRP* 37(2–4), 1–332.
- [3] Papworth, D.S. (1997) A need to reduce the radon gas hazard in the UK. *J. R. Soc. Health*. 117, 75–80.
- [4] Coskeran, T., Denman, A., Phillips, P., Gillmore, G. & Tornberg, R. (2006) A new methodology for cost-effectiveness studies of domestic radon remediation programmes: quality-adjusted life-years gained within primary care trusts in Central England. *Sci. Total Environ*. 366, 32–46.
- [5] Gillmore, G.K., Phillips, P., Denman, A., Sperrin, M. & Pearce, G. (2001) Radon levels in abandoned metalliferous mines, Devon, Southwest England, *Ecotoxicol. Environ. Saf.* 49, 281–292.
- [6] Gillmore, G., Gilbertson, D., Grattan, J. et al. (2005) The potential risk from radon-222 posed to archaeologists and earth scientists: reconnaissance study of radon concentrations, excavations and archaeological shelters in the Great Cave of Niah, Sarawak, Malaysia. *Ecotoxicol. Environ. Saf.* 60, 213–227.
- [7] Phillips, P.S., Denman, A.R., Crockett, R.G.M., Gillmore, G., Groves-Kirkby, C.J. & Woolridge, A. (2004) Comparative Analysis of Weekly vs. Three Monthly Radon Measurements in Dwellings. DEFRA Report No., DEFRA/RAS/03.006. DEFRA, London.
- [8] Cliff, K. & Gillmore, G.K. (eds.) (2001) *The radon manual: a guide to the requirements for the detection and measurement of natural radon levels. Associated Remedial Measures and Subsequent Monitoring of Results*, 3rd edn. The Radon Council, Shepperton, Middlesex, U.K.
- [9] Petford, N., Wertheim, D. & Miller J.A. (2005) Radon track imaging in CR-39 plastic detectors using confocal scanning laser microscopy. *J. Microsc.* 217, 179–183.
- [10] Naismith, S.P., Howarth, C.B. & Miles, J.H.C. (1998) Results of the 1997 European Commission Intercomparison of Passive Detectors. EUR 18035 EN. European Commission, Brussels.
- [11] Henshaw, D.L., Allen, J.E., Keitch, P.A. & Randle, P.H. (1994) Spatial distribution of naturally occurring ^{210}Po and ^{226}Ra in children's teeth. *Int. J. Radiat Biol.* 66, 815–826.
- [12] Nikezic, D. & Yu K.N. (2008) Computer program TRACK_VISION for simulating optical appearance of etched tracks in CR-39 nuclear track detectors. *Comput. Phys. Comm.* 178, 591–595.
- [13] Wagner, W. & Van Der Haute, P. (1992) *Fission Track Dating*. Kluwer Academic Publishers, Dordrecht.
- [14] Fleischer, R.L., Price, P.B. & Walker, R.M. (1975) *Nuclear Tracks in Solids: Principles and Applications*. University of California Press, Berkeley, California.
- [15] Gonzalez, R.C. & Woods, R.E. (2002) *Digital Image Processing*, Second edn, Prentice Hall, New Jersey.
- [16] Kanthathas, K., Willmot, D.R. & Benson, P.E. (2005) Differentiation of developmental and post-orthodontic white lesions using image analysis. *Eur. J. Orthod.* 27, 167–172.

02 Application of confocal microscopy for surface and volume imaging of solid-state nuclear track detectors

D. Wertheim, G. Gillmore

SUMMARY

Inhalation of radon gas is considered a risk factor in the development of lung cancer. Solid-state nuclear track detectors (SSNTDs) are often used for monitoring radon levels. We have previously shown that 3D imaging can help distinguish real tracks from artifacts. In this study, we investigated particle tracks in nine SSNTDs using surface and volume visualization from confocal microscope imaging. An Olympus LEXT™ OLS4000 confocal microscope equipped with the Olympus LEXT Remote Development Kit was used to acquire z-stack images and surface data from the SSNTDs. Surface and volume visualization analysis methods were developed and applied to examine the data. The mean (standard deviation) depth of 45 tracks from the nine detectors was 9.5 (4.6) μm . The mean difference in track depth using the two analysis techniques was 0.08 μm , thus showing good agreement. Furthermore, volume visualization should enable assessment of the structure of tracks deep in the detector.

BACKGROUND

As outlined on pp. 6–7 of this eBook, the inhalation of radon gas has been shown to be a risk factor in the development of lung cancer^[1]. It is estimated that there are 1,100 home radon-related lung cancer deaths annually in the United Kingdom alone^[2]. Radon levels can be measured using small etched plastic detectors called solid-state nuclear

track detectors (SSNTDs); the detectors are often based on poly-allyl-diglycol carbonate or PADC, commercially known as CR-39.

CR-39 detectors

SSNTDs are more similar to human tissue than other passive detectors^[3]. They are extensively used in dosimetry because of their low linear energy transfer (LET) threshold for detection of charged particles^[4], hence their use

in measuring radon and its decay products in buildings. SSNTDs are also used in neutron dosimetry and the neutron response of such detectors has relied on the simulation of the formation/development of etched tracks as a function of energy and etching time^[5]. Some authors have undertaken simulated 3D computation of track shape in order to better understand the potential effect of incidence direction of charged particles and SSNTD track development^[6,7]. The measurement of track parameters then can provide data on the energy deposition of the incident particle^[3], and analysis of tracks produced by α particles, protons, or nuclear fission fragments is a very valuable tool^[8]. The geometry of α -track cone formation in SS-NTDs can provide information on energy and charge and direct measurements of track lengths are sometimes required^[8]. The α -track etch-pit diameters can act as a spectrometer in that they can be related to incident α energy^[9]. In one study, detectors were broken in order to make direct measurements of the track length^[7], while others have utilized atomic force microscopy (AFM), but due to probe geometry the bottom of the track has not been reached^[8]; a holographic technique in combination with an interferometer has also been applied to obtain surface views of tracks^[8]. Thus, there have been few studies imaging actual track depths using nondestructive techniques.

SSNTD imaging

Conventionally etched SSNTDs are assessed using 2D microscope imaging. Confocal microscopy can be used to obtain 3D image datasets of tracks in SSNTDs^[10,11]. Fluorescent confocal microscopy was used to image SSNTDs by treating the detectors with Nile Blue A^[10]. We have previously used the LEXT™ OLS3100 confocal microscope to successfully image CR-39 radon track detectors^[11-13]. These studies used reflection confocal microscopy to enable 3D visualization and quantification of tracks from surface data without the need for using a fluorescent dye. A recent addition to the LEXT™ OLS4000 microscope enables z-stack images to be stored in addition to the acquisition of surface image data. Hence, this potentially allows examination of 3D material structure around tracks which may help in the interpretation of coalescing and angled tracks.

AIM

The aim of this study was to investigate single and coalescing particle tracks with sur-

face and volume visualization of confocal microscope SSNTD image datasets.

METHOD

Nine CR-39 plastic radon detectors previously exposed in rooms, or a controlled radon chamber were processed by etching for up to 4.5 hours in 6M NaOH solution at 90 °C (194 °F) in the KU (Micro) Radon Laboratory at Kingston University; the etching conditions could potentially affect the microscopic appearance of tracks. The etched SSNTDs were cleaned with distilled water in an ultrasonic bath for 2 minutes. Detectors were individually placed on the microscope stage of an Olympus LEXT™ OLS4000 confocal microscope (Olympus Corporation, Japan). The microscope system was equipped with the Olympus LEXT Remote Development Kit (RDK), thus allowing acquisition of z-stack images as well as surface imaging. The detectors were

initially examined using the LEXT operating in 2D imaging mode using 5X and 10X objective lenses followed by 3D scanning using the standard 'fine' surface scanning mode (with 'Color'); the method is similar to that used in earlier studies with an OLS3100 microscope^[12,13]. In confocal mode, 50X or 100X objective lenses were used (NA 0.95), and the microscope has a 405 nm laser. The images were acquired with a size of 1024 × 1024 pixels; using the 50X lens, the xy area imaged was 260 × 260 μm , thus giving a lateral spatial resolution of 0.25 μm per pixel. Before scanning, the top (upper detector surface) and bottom levels were determined manually. 2D and 3D screenshots were acquired as single image files. Heightmap data were downloaded in a spreadsheet-compatible file in order to allow subsequent 3D visualization and analysis.

In this study, we examined and compared surface data with z-stack imaging. The surface data were analyzed from the heightmap spreadsheets. Z-stack imaging was obtained using the LEXT RDK, and hence it is possible to enable volume visualization from the confocal slices.

Script files were written for the RDK to run on the controlling PC in order to allow appropriate movement of the objective lens following each z-slice acquisition; in each script file, movement was set such that the objective lens moved up away from the slide in 0.1 μm steps. As the top and bottom posi-

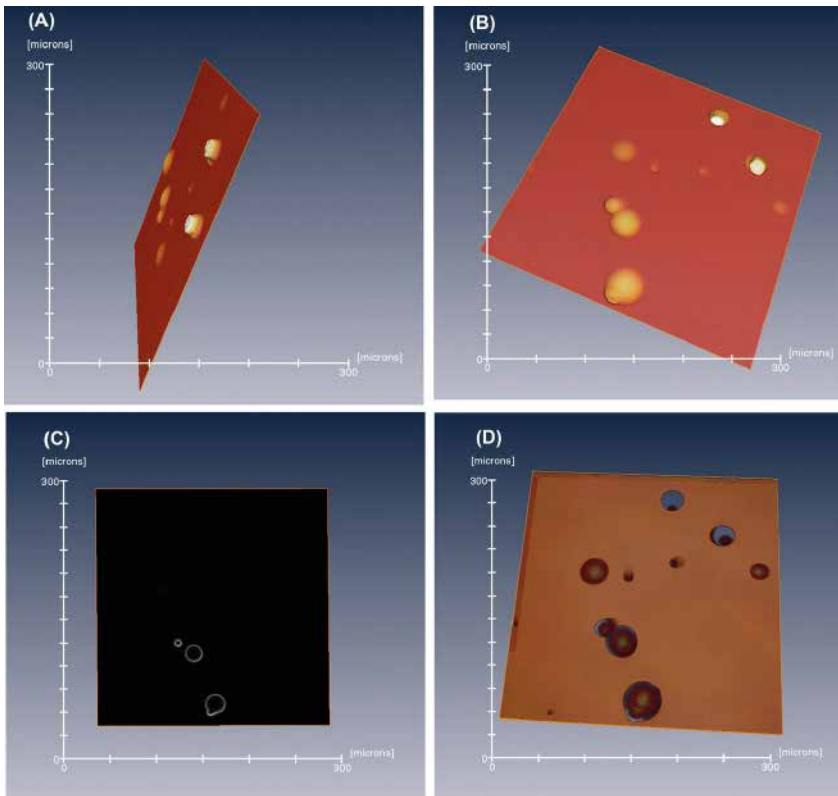


Figure 1: Example showing 3D surface imaging (50X objective) from height data with LEXT microscope; (A) shows a side view from the lower side of the detector, (B) shows 3D surface from top surface, (C) shows an example of a single z-stack intensity image an example of a stack intensity image, and (D) shows 3D volume visualization of tracks from a z-stack dataset. In each image the lengths of the abscissa and ordinate axes are 300 μm .

tions were known, the number of slices to be acquired could be calculated, and hence the number of slices to be collected was set in the script file; the z-stack images were collected.

3D visualization

Software was written in MATLAB (The MathWorks Inc., Natick, MA, U.S.A.) in order to read the height field map spreadsheet files. The mode height was calculated to determine the level of the detector surface. The minimum and maximum heights were computed, and the data was remapped as a gray scale image covering the full range of height values. The resultant images were read into Amira v. 5.4 (VSG, Visualization Sciences Group), and networks were developed to allow examination of the 3D visualization. Further software was developed in MATLAB in order to display surface data and compute the distribution of track depths.

Surface and volume visualizations of the z-stack images were also performed using Amira; iso-surface and vortex visualization techniques were applied to examine the image data.

Comparison of track depths

Track depths calculated from the surface spreadsheet files were compared with the stack data for 45 tracks in the nine detectors. In Amira, the depth of the tracks was examined using orthoslice visualization; in this mode, the signal from the confocal microscope imaging can easily be seen in successive z-slice images, and an example can be seen in **Figure 1C**. The track depths were thus calculated from the difference between the detector surface level and the lower surface of each of the tracks as the distance between slices is constant; the lower surface was defined as the lowest position where the track is discernible. Data were tested for consistency with a normal distribution using the Ryan–Joiner test in Minitab v. 16 (Minitab Inc., U.S.A.).

RESULTS

Visualization using 3D surface and volume approaches were compared. **Figure 1** shows an example of surface imaging from depth data in comparison with volume visualization. The Figure shows views from the lower side of the detector and looking from the top surface. This is compared with volume visualization (**Figure 1D**) formed by combining the z-stack of intensity images, one of which is shown in **Figure 1C**. The techniques applied for volume visualization of the stack data did not apply connection of surfaces so that the raw intensity data were used; this can result in apparent gaps but avoids potential difficulties from applying assumptions about surface geometry.

Figure 2 shows an example of zooming in on an angled track as well as two apparently very closely coalescing tracks. The volume visualization technique allows zooming in to examine the surface in more detail, thus identifying the likely closely coalescing tracks and the appearance of an angled track. These examples illustrate that visualization of z-stack data enables structure of the tracks deep in the detector to be seen. An example of the analysis of track depth data using software we developed in MATLAB is shown in **Figure 3**. Using data from another detector, the representation of depth in a gray scale or pseudocolor image helps to assess the depth of each individual track with respect to the detector surface. Tracks 1, 2,

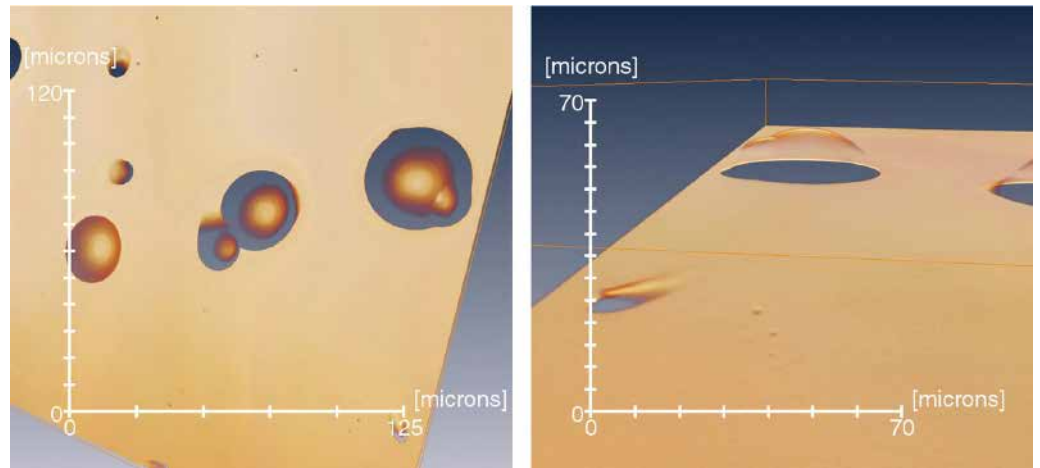


Figure 2: Example showing zoomed visualization of **Figure 1** stack imaging. The left-hand image shows a view of the top surface and the right-hand image shows an image viewed from deep in the detector to the top surface.

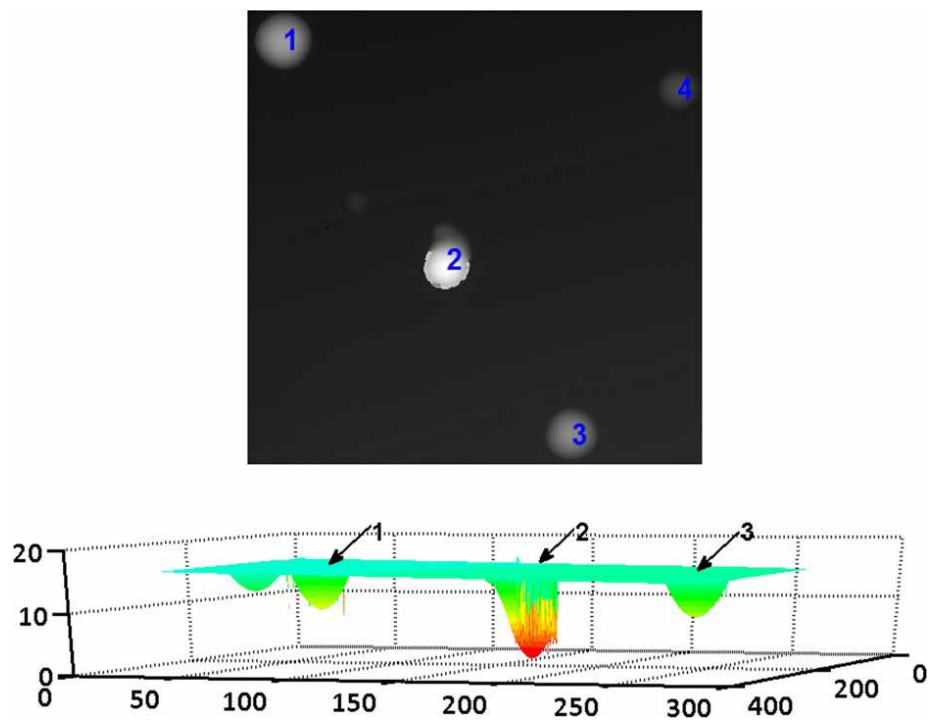


Figure 3: An example of a depiction of track depth data using a greyscale image (upper). The lower part of the figure shows a 3D representation of the data.

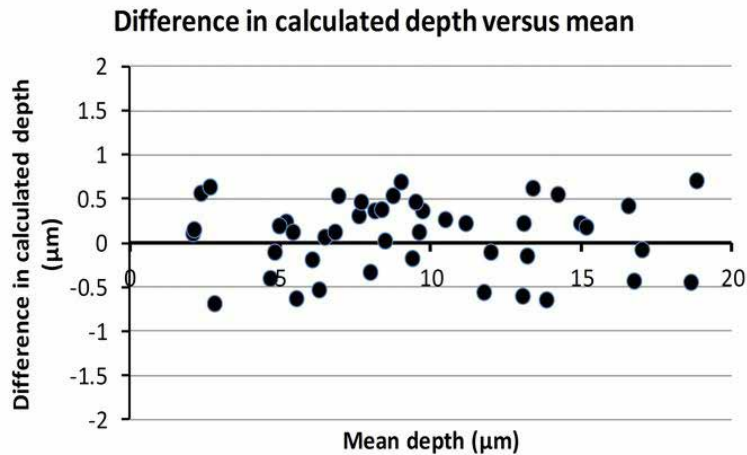


Figure 4: Graph showing the difference in calculated depth (surface measured depth – stack measured depth) plotted against the mean of the two measurements.

and 3 have depths of 7.5, 14.5, and 6.6 μm , respectively, as can be seen in the lower part of the figure with a 3D representation obtained using software we developed in MATLAB.

Comparison of track depths

The mean (standard deviation) depth of the 45 tracks was 9.5 (4.6) μm . **Figure 4** shows a graph of the difference in calculated depth (surface depth minus stack measured depth) against the mean in accordance with a method for comparing measurements^[14]. The mean (standard deviation) difference in calculated depths between the two methods was 0.08 (0.40) μm . There was no significant correlation between the difference in the two measurements and the mean (Pearson's correlation coefficient $r = -0.02$, $p = 0.9$). The depths are consistent with previous observations^[13].

DISCUSSION

Assessment accuracy is important not only for radon detection and remediation but also for dosimetry. Coalescing tracks may cause problems of interpretation using conventional 2D analysis, these difficulties could be addressed using 3D imaging which also helps to distinguish real tracks from artifacts; artifacts due to dust or similar particles should be evident by protrusion above the top surface. Coalescing tracks are likely to be particularly evident with high track densities associated with high radon concentrations.

Detection of surface features has wide applications in material analysis. In the case of SSNTDs, surface tracking may be difficult for very steep tracks that could occur in some deep and angled tracks. Furthermore, coalescing tracks could be difficult to assess because of the associated complex profile. Z-stack imaging allows the raw data to be displayed, thus avoiding possible artifacts that may be seen in steep, angled tracks; furthermore, the method allows a detailed view of the structure of coalescing tracks. Hence, 3D imaging allows examination of coalescing tracks and helps to discern real tracks from artifacts, both of which potentially could be problematic in 2D analysis. The examples in **Figures 1** and **2** illustrate that visualization of z-stack data images allows examination of the structure of tracks deep in the detector.

Rather than only imaging the surface, in transparent and partially transparent materials, stack imaging should allow examination around the surface into the material. Thus, we have been able to study the structural appearance of tracks. Additional information can possibly be obtained regarding surfaces associated with steep angles with respect to the upper surface. The stack imaging system enables examination of the reflected signal, thus allowing detailed interpretation of the data associated with steep angular features as can be seen, for example, in deep tracks and certain angled tracks. In addition, if 3D surface imaging identifies unexpected surfaces, stack imaging can help in the interpretation of data in order to understand better the resultant visualization. The comparison of calculated depths using the two techniques showed good agreement.

CONCLUSIONS

Series of z-stack images were acquired using the Olympus LEXT™ RDK as well as surface imaging data with the microscope and software was developed to enable 3D visualization and analysis of the data in order to examine radon tracks in CR-39 detectors. Stack imaging can enable visualization that complements conventional 3D surface imaging as it allows examination of the material surrounding the detected surfaces. Comparing the two analysis techniques, there was good agreement in the calculated measurement of track depth. This approach should enable the assessment of the structure of tracks deep in the detector, which could help in the interpretation of images and hence improve SSNTD assessment.

REFERENCES

- [1] Darby, S., Hill, D., Auvinen, A., et al. (2005) Radon in homes and risk of lung cancer: collaborative analysis of individual data from 13 European case-control studies. *Br. Med. J.* 330, 223–228.
- [2] Gray, A., Read, S., McGale, P. & Darby, S. (2009) Lung cancer deaths from indoor radon and the cost effectiveness and potential of policies to reduce them. *Br. Med. J.* 338, 215–218.
- [3] Caresana, M., Ferrarini, M., Fuerstner, M. & Mayer S. (2012) Determination of LET in PADC detectors through the measurement of track parameters. *Nucl. Instr. Methods Phys. Res. A* 683, 8–15.
- [4] Lounis, Z., Djefal, S., Morsli, K. & Allab, M. (2001) Track etch parameters in CR-39 detectors for proton and alpha particles in different energies. *Nucl. Instr. Methods Phys. Res. B* 179, 543–550.
- [5] Dörschel, B., Bretschneider, R., Hermsdorf, D., Kadner, K. & Kühne, H. (1999) Measurement of the alpha track etch rates along proton and alpha particles trajectories in CR-39 and calculation of detection efficiency. *Rad. Measur.* 31, 103–108.
- [6] Azooz, A.A., Hermsdorf, D. & Al-Jubbori, M.A. (2013) New approach of modeling charged particles track development in CR-39 detectors. *Rad. Measur.* 58, 94–100.
- [7] Dörschel, B., Hermsdorf, D., Reichelt, U., Starke, S. & Wang, Y. (2003) 3D computation of the shape of etched tracks in CR-39 for oblique particle incidence and comparison with experimental results. *Rad. Measur.* 37, 563–571.
- [8] Palacios, F., Palacios Fernández, D., Ricardo, J., Palacios, G.F., Sajo-Bohus, L., Goncalves, E., Valin, J.L. & Monroy, F.A. (2011) 3D nuclear track analysis by digital holographic microscopy. *Rad. Measur.* 46, 98–103.
- [9] Soares, C.J., Alencar, I., Guedes, S., Takizawa, R.H., Smilgys, B. & Hadler, J.C. (2013) Alpha spectrometry study on LR115 and Makrofol through measurements of track diameter. *Rad. Measur.* 50, 246–248.
- [10] Hermsdorf, D. & Hunger, M. (2009) Determination of track etch rates from wall profiles of particle tracks etched in direct and reversed direction in PADC CR-39 SSNTDs. *Rad. Measur.* 44, 766–774.
- [11] Petford, N., Wertheim, D. & Miller, J. (2005) Radon track imaging in CR-39 plastic detectors using confocal scanning laser microscopy. *J. Microsc.* 217, 279–283.
- [12] Wertheim, D., Gillmore, G., Brown, L. & Petford, N. (2010a) A new method of imaging particle tracks in Solid State Nuclear Track Detectors. *J. Microsc.* 237, 1–6.
- [13] Wertheim, D., Gillmore, G., Brown, L. & Petford, N. (2010b) 3-D imaging of particle tracks in solid state nuclear track detectors. *Nat. Haz. Earth Syst. Sci.* 10, 1033–1036.
- [14] Bland, J.M. & Altman, D.G. (1986) Statistical methods for assessing agreement between two methods of clinical measurement. *Lancet* 1(8476), 307–310.

03 Application of confocal microscopy for 3D visualization of tracks in solid-state nuclear track detectors

D. Wertheim, G. Gillmore

ABSTRACT

Inhalation of radon gas is considered to be associated with about 1,100 people dying annually from lung cancer in the UK alone. Accurate and timely assessment of radon levels is thus important in areas with known elevated radon level risk in order to be able to institute remedial procedures. A common method for monitoring radon concentration is with small plastic detectors known as solid-state nuclear track detectors (SSNTDs). This paper reviews recent research in 3D imaging of SSNTDs using confocal microscopy.

INTRODUCTION

Inhalation of radon gas, that is ^{222}Rn and its associated radioactive heavy metallic daughter products such as ^{214}Po , is estimated to be associated with about 1,100 lung cancer-related deaths annually in the UK^[1-3] and 21,000 in the USA^[4]. Furthermore, radon exposure can increase the risk of lung cancer in smokers as well as non-smokers^[5]. The gas is a natural hazard that can be found in elevated levels in areas of the UK as well overseas; it is formed as a result of the natural radioactive breakdown of uranium ^{238}U present in rocks and soils. Radon gas is colorless and odorless, so its presence could remain undetected without the use of appropriate sensing technology. It is possible for concentrations to become unsafe, for example in poorly ventilated rooms, mines, and caves^[6]. Amelioration in both homes and workplaces by adequate room ventilation measures may thus be required in order to

reduce radon levels in affected areas^[7]. Hence, monitoring radon concentrations in buildings is routinely undertaken in certain areas with the potential for elevated radon levels.

Measurement of radon levels in buildings is thus an important step toward tackling increased radon gas levels in rooms inhabited by humans. Solid-state nuclear track detectors (SSNTDs) are small passive devices often made of plastic that can be used to measure radon concentrations in the atmosphere. They are commonly placed in an outer enclosure that ensures air passes over the detector. Alpha particles formed by the nuclear breakdown of radon cause tiny sub-microscopic indentations, termed tracks, in the SSNTD. In order to make these visible for a light microscope, the detectors are etched. Radon gas concentration can be measured with CR-39 plastic detectors^[8], but even detectors near each other can give differing readings^[6]. CR-39 solid-state

nuclear track-etch detectors are the most commonly used for radon gas measurements.

Typically, the detectors are placed in rooms for several weeks. In order to make tracks in the SSNTD from alpha particles visible with a microscope, the tracks are enlarged using a process called etching, but this can vary in time, temperature, and etchant concentration. The standard method of assessing radon concentration involves analysis of 2D microscope images of the SSNTDs; using this approach, tracks often appear circular or elliptical in cross-section. However, distinguishing real tracks from artifacts using 2D imaging and analysis alone can be difficult.

Radon concentrations are derived from counting the number of tracks seen in SSNTDs exposed for a given period. The tracks are conventionally counted by image analysis of 2D microscope images of the detector. The length of time of the etching process can affect the size of the tracks seen^[9]. This potentially could affect the counting process as short etching times could result in small tracks that may be difficult to discern, whereas long etching times could result in coalescing tracks from which it could be difficult to discern individual tracks as well as distinguishing real tracks from artifacts. Thus, etching times are important to consider as well as similarly etching temperature and pH.

DEVELOPMENTS IN MICROSCOPE IMAGING OF RADON TRACKS

Confocal microscopy has previously been used to examine fission tracks in mica and apatite^[10]. We have developed and applied methods for 3D image analysis and visualization of radon tracks in SSNTDs using confocal microscopy^[9,11-14]. There can be some variation in track diameters; the results from a study indicated that the typical median (range) equivalent track diameter for single tracks is 46.1 (20.05 to 62.44) μm for standard processing^[12,13]. In our studies, Olympus LEXT™ confocal microscopes have been used to image tracks, and the results have shown that tracks can have different sizes, shapes, and angles. In addition, we identified that tracks in close proximity can coalesce into a cluster; such clusters could potentially be difficult for 2D image analysis to distinguish from artifacts. 3D imaging allows a clearer distinction of real tracks from artifacts compared with 2D imaging as

the full 3D extent can be ascertained from the visualization rather than just a surface image. Thus, we suggest that 3D imaging and analysis may help to improve measurement accuracy.

COMPARISON OF 2D AND 3D IMAGING

In our studies, we have used LEXT™ models OLS3100, OLS4000, and OLS4100 confocal laser scanning microscopes (Olympus Corporation, Tokyo, Japan) to acquire 3D image data on CR-39 plastic detectors as previously described^[9,12-14]; the detectors used were from the Radon Metrology Laboratory at Kingston University. The detectors were placed on a glass slide or directly on the microscope stage. Confocal microscope images were obtained primarily using a 50X or 100X objective mostly in fine mode; both lenses had a numerical aperture (NA) of 0.95. Examples comparing 2D imaging with 3D imaging are shown in **Figures 1 to 3**. **Figure 1** shows an example of an artifact caused by debris on the surface that can be seen to be easily identified with 3D imaging as it lies above the surface, whereas it could potentially be confused with a small track using 2D imaging alone.

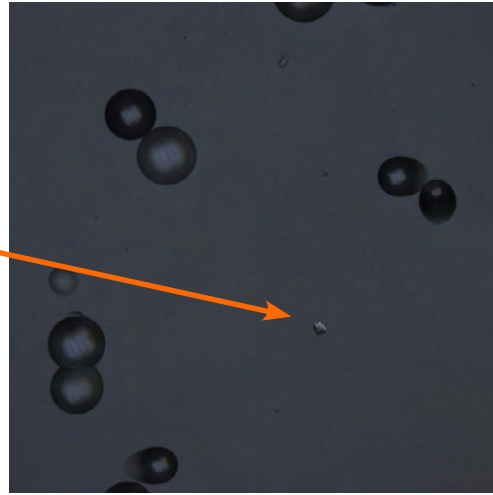
Figure 1 shows a 2D image of an SSNTD. From the image one bright area could be a small track or artifact. 3D imaging shows that it is indeed an artifact as seen in **Figures 2** (right-hand image) and **3** since it emanates above the detector surface.

Depending on radon concentration and length of exposure of the detector, tracks can occur in close proximity to other tracks on the SSNTD. If tracks coalesce, it is possible that a basic 2D imaging and analysis system could have a tendency to count such multiple strikes as one or as an artifact if not of circular appearance. With longer exposures or higher radon concentrations, there is an increased likelihood that tracks could overlap or be superimposed on one another. If tracks coalesce it is possible that individual tracks may be difficult to detect using 2D image analysis, and there may thus be the potential for underassessment of track numbers; 3D imaging allows detailed examination of coalescing tracks, which could thus help in situations where SSNTDs are used over long periods or in high radon concentrations.

Our studies with the Olympus LEXT microscope have shown that confocal microscopy can be used to examine SSNTD tracks

EXAMPLE IMAGES

Figure 1: 2D image of an SSNTD using a 50X objective lens. Scale 257 by 257 μm . Blue arrow indicates an area that appears to be an artifact or a small track.



in 3D^[9,12]. Suitable specimen and slide preparation are important as had helped in applying the techniques to other fields of study, such as imaging of volcanic ash particles^[15].

CONCLUSIONS

Radon measurement is a key step in identifying whether levels of this colorless, odorless, radioactive gas could pose a risk to human health. A number of measurement methods are available, and one of the simplest to use is with SSNTDs. SSNTDs require no power supply and minimal maintenance and so are ideal for use around buildings as well as in remote areas. Part of our current research involves investigating if SSNTD measurement accuracy can be improved using 3D microscopy imaging compared with 2D imaging. Our results suggest that 3D imaging of radon tracks can help to enable distinguishing artifacts from real tracks; in particular 3D imaging helps to clearly identify features on the surface of the detectors that 2D imaging would not be able to easily characterize. Additionally, 3D imaging helps in the identification of multiple coalescing tracks, which are a particular issue in detectors with a high number of tracks and may have complex shapes; if the image detection is based solely on detecting round shapes, there could be a possibility for underassessment of the number of tracks. Confocal imaging enables the number of contributing tracks in coalescence to be examined closely as well as distinguishing real tracks from artifacts. Thus, 3D imaging may help in improving the accuracy of track determination in SSNTDs.

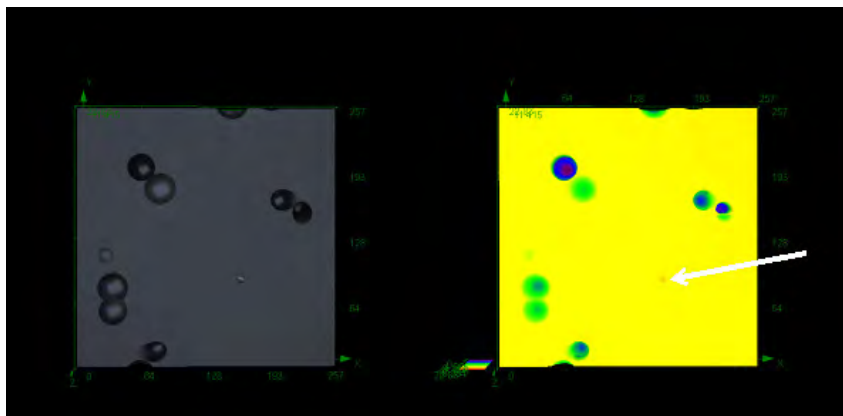


Figure 2: Equivalent 3D images showing detection of an artifact (orange, indicated with white arrow) above the level of the track in yellow. The left image shows a color view with a true color representation, whereas the right-hand image is color encoded for height with blue/violet being the deepest and red the highest level; the surface of the detector is thus in yellow.

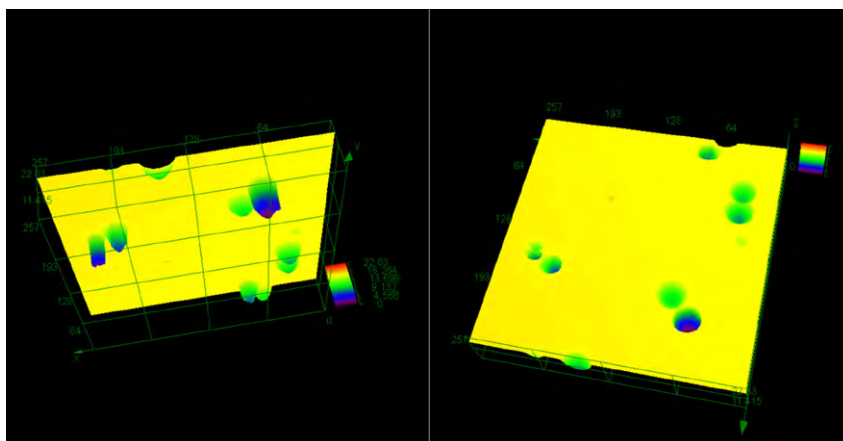


Figure 3: Alternative 3D views of the same detector with color-coded height, i.e., blue/violet being the deepest and red the highest level; the surface of the detector is yellow.

REFERENCES

- [1] Darby S., Hill D., Auvinen A., Barros-Dios JM., et al. Radon in homes and risk of lung cancer: collaborative analysis of individual data from 13 European case-control studies. *BMJ*. 2005 Jan 29;330(7485):223. doi: 10.1136/bmj.38308.477650.63.
- [2] Gray A, Read S, McGale P, Darby S. Lung cancer deaths from indoor radon and the cost effectiveness and potential of policies to reduce them. *BMJ*. 2009 Jan 6;338:a3110. doi: 10.1136/bmj.a3110.
- [3] ICRP, 2007. *The 2007 Recommendations of the International Commission on Radiological Protection*. ICRP Publication 103. Ann. ICRP 37 (2-4). <https://www.icrp.org/publication.asp?id=ICRP%20Publication%20103> (accessed 31st January 2022).
- [4] Environmental Protection Agency (EPA), 2003. *EPA Assessment of Risks from Radon in Homes*. Office of Radiation and Indoor Air, United States Environmental Protection Agency, EPA Report 402-R-03-003, Washington DC, USA. <https://www.epa.gov/sites/default/files/2015-05/documents/402-r-03-003.pdf> (accessed 31st January 2022).
- [5] Torres-Durán, M., Ruano-Ravina, A., Pariente-Lamelas, I, Leiro-Fernández, V., et al. Lung cancer in never-smokers: a case-control study in a radon-prone area (Galicia, Spain). *Eur Respir J*. 2014 Oct;44(4):994-1001. doi: 10.1183/09031936.00017114.
- [6] Cliff K, Gillmore GK. (Eds.), 2001. *The Radon Manual: A Guide to the Requirements for the Detection and Measurement of Natural Radon Levels. Associated Remedial Measures and Subsequent Monitoring of Results*, 3rd Edition. The Radon Council, Shepperton, Middlesex.
- [7] Health and Safety Executive, 2010. *Radon in the workplace*, <http://www.hse.gov.uk/radiation/ionising/radon.htm> (accessed 31st January 2022).
- [8] Phillips PS, Denman AR, Crockett RGM, Gillmore G, Groves-Kirkby CJ, Woolridge A, 2004. *Comparative Analysis of Weekly vs. three monthly radon measurements in dwellings*. DEFRA Report No., DEFRA/RAS/03.006.
- [9] Gillmore G, Wertheim D, Crust S. Effects of etching time on alpha tracks in solid state nuclear track detectors. *Sci Total Environ*. 2017 Jan 1;575:905-909. doi: 10.1016/j.scitotenv.2016.09.147.
- [10] Petford N, Miller JA. The study of fission tracks and other crystalline defects using confocal scanning laser microscopy. *Journal of Microscopy*. 1993; 170: 201–212.
- [11] Petford N, Wertheim D, Miller JA. Radon track imaging in CR-39 plastic detectors using confocal scanning laser microscopy. *J Microsc*. 2005 Mar;217(Pt 3):179-83. doi: 10.1111/j.1365-2818.2005.01444.x.
- [12] Wertheim D, Gillmore G, Brown L, Petford N. A new method of imaging particle tracks in solid state nuclear track detectors. *J Microsc*. 2010 Jan;237(1):1-6. doi: 10.1111/j.1365-2818.2009.03314.x.
- [13] Wertheim D, Gillmore G, Brown L, Petford N. 3-D imaging of particle tracks in solid state nuclear track detectors. *Natural Hazards and Earth System Sciences*. 2010; 10: 1033–1036. <https://doi.org/10.5194/nhess-10-1033-2010>.
- [14] Wertheim D, Gillmore G. Application of confocal microscopy for surface and volume imaging of solid state nuclear track detectors. *J Microsc*. 2014 Apr;254(1):42-46. doi: 10.1111/jmi.12114.
- [15] Wertheim D, Gillmore G, Gill I, Petford N. High resolution 3D confocal microscope imaging of volcanic ash particles. *Sci Total Environ*. 2017 Jul 15;590-591:838-842. doi: 10.1016/j.scitotenv.2017.02.230.